J. Fluid Mech. (1991), *vol.* 229, *pp.* 629–657
Printed in Great Britain

Surface current and recirculating cells generated by bubble curtains and jets

By T. K. FANNELØP, S. HIRSCHBERG AND J. KÜFFER
Swiss Federal Institute of Technology, Sonneggstrasse 3, CH-8092 Zürich, Switzerland

(Received 23 July 1990)

The flow structure associated with a line bubble plume in shallow water is investigated. G. I. Taylor has proposed the use of such plumes as wavebreakers. To be effective the surface current generated should be stable for a distance of the order of the wavelength, which in turn could be several times the depth. It appears that the formation of recirculating cells can affect the wavebreaking potential of line bubble plumes. The paper presents observations and measurements of the cell structure associated with line bubble plumes as obtained in a model towing basin of dimensions $1 \times 1 \times 40$ m. A recirculating region was found on both sides of the plume, but the secondary (and higher-order) cell structures proposed by other investigators were not observed. The primary cells were found to be appreciably longer than those reported in the literature for vertical plane jets. The difference can in part be attributed to different definitions of cell length. The definitions used herein are based on observables, both on the water surface and in the interior of the flow, and they lead to consistent measures of length. Bubble-plume parameters (such as entrainment coefficient) are known to depend on gas flow rate, and it was found that the length of the primary cell is a weak function of this variable as well. Additional experiments with a vertical plane jet were conducted for comparison. Longer cells than those previously reported were again observed. The paper contains a complete theory for line bubble plumes, including the effects of compressibility, bubble slip and finite release volume, as well as a simplified similarity analysis useful in estimating plume properties and horizontal-current depth and velocity.

1. Introduction

Two-dimensional underwater bubble plumes or bubble curtains, are now being promoted for many practical purposes, e.g. as 'pneumatic' oil barriers, for aeration in stagnant waters, for destratification of reservoirs, and to prevent ice formation in lakes and harbour basins. Large-scale use of bubble plumes as breakwaters, based on the work of Taylor (1955), has not materialized owing to the high energy requirements as estimated by Bulson (1968) and others. The protection of coastal or offshore structures from an occasional storm can hardly justify the large installation of compressors and piping required to damp the waves. But the surface current that damps the waves could have other beneficial effects; one possibility would be to deflect large drifting objects (floating ice, ships out of control), away from vulnerable structures, such as oil and gas production platforms.

If a large high-pressure supply of gas is already available, its occasional use for safety purposes requires only an additional and perhaps marginal investment in valves and piping. Such very large gas supplies are often available near offshore

installations in the form of a gas reservoir, a long high-pressure pipeline or a nitrogen production plant for gas injection in a depleted reservoir. A recent project study indicated that a source strength per metre of one normal cubic metre per second would be possible for a major offshore petroleum platform. This suffices to produce a current of 10 m depth and 5 m/s peak velocity at a distance 50 m from the plume baseline for depths typical of North Sea installations.

It is tacitly assumed, in all discussions of large-scale applications, that the depth of the outward-directed current, generated by the plume, is much less than the ocean depth. The current is furthermore assumed to be unlimited in extent. The offshore or coastal installations in need of protection are normally found in waters of moderate depths, typically only a fraction of the wavelength of the critical wave. But cursory calculations of the depth of the surface current, based on available information on bubble-plume flow and on surface-jet entrainment rates, indicate that this depth approaches the typical ocean depth at distances of the order of a wavelength from the bubble plume, clearly an impossible flow configuration (for reasons of continuity). The mass flow towards the plume at lower depths must equal that of the outflowing surface current, and to maintain a two-dimensional flow we need some kind of a recirculating cell. Thermal stratification plays a role as well, the bottom water which is lifted to the surface by the plume is often cold and this promotes the formation of cells.

The problem of cell formation in shallow waters as a result of a vertical plane-jet discharge was considered by Jirka & Harleman (1979), further theoretical discussions are given by Jirka (1982) and supplementary experimental results have been supplied by Andreopoulos, Praturi & Rodi (1986). There is little reason to believe that bubble plumes and vertical jets of equal mass and momentum flux will produce widely different flow configurations. This also has implications for the large-scale utilization of bubble plumes as proposed in the past. The extent of the primary cell for a non-buoyant discharge was estimated by Jirka & Harleman to be about 2.5 times the depth. Carried over to the case of a plume, this means that the extent of the surface current in many interesting cases will be less than half the wavelength of the design wave. This does not necessarily invalidate Taylor's idea, but it indicates a need for modification of the theory. There are implications for experimental work as well. The testing of proposed large-scale applications of bubble plumes will have to be undertaken in existing maritime test facilities, such as ship model tanks. These have closed endwalls, which could affect the cell size and flow character.

Our paper presents the theory required to predict the plume and surface flow associated with line sources. General but approximate solutions of similarity form are developed for both flows, and these solutions are considered adequate for most practical applications outside the laboratory. On accounting for velocity slip and other effects associated with real bubble plumes, the problem becomes non-similar. The full problem with all relevant terms included has been solved numerically to assess the accuracy and validity of the general similarity solution.

The problem of cell formation has been studied in two ways; by reviewing existing information, particularly field observations, and by conducting experiments in an available laboratory facility, a small towing tank. Although this channel is small in comparison with that required for realistic simulation, it is much larger in physical dimensions than the near identical flow arrangements used by Jirka & Harleman and by Andreopoulos *et al.*

2. Known observations from large-scale plumes

The only large-scale experiment with two-dimensional bubble plumes known in the literature is that of Bulson (1963). The test tank used had a depth of 25 ft (the source depth was slightly less), a length of 1300 ft and a width of 48 ft. Measurements of the surface current (in the absence of waves) were made at distances up to 60 ft (i.e. about 2.5 times the depth), where the velocity was found to be about 5% of the initial (maximum) value. This does not contradict the idea of a cell structure. Measurements of the incident-wave height in the current showed a gradual increase starting from a distance of 160 ft (wavelength 30.75 ft) or about 6 times the depth. This could indicate a primary cell much larger than that suggested by Jirka & Harleman. As the second cell would have a current direction which would reduce rather than increase the wave height, it would appear that the primary cell is either very long as indicated or that the cell structure breaks down in the presence of waves of sufficient strength.

More recent large-scale experiments with bubble plumes have been motivated by underwater blowouts; i.e. offshore oil or gas wells blowing out of control. Such an event gives rise to an axisymmetric bubble plume and a radial current directed outward from the so called 'boil region' on the surface. The oil from a blowout will be transported outward by this current, at a rate much faster than oil released from, say, a tanker accident (Fanneløp & Sjøen 1980). According to Jirka (1982) we can also expect recirculating cells for vertical axisymmetric jets for certain combinations of depth to jet-diameter ratio and Froude number. From his large-scale field experiments with bubble plumes at source depths down to 60 m, Topham (1975*a*, *b*) reported the observation of a 'wavering' on the surface. This 'wavering' (in effect a stagnation line) separated the outward-directed surface current from a secondary inward current, and, in the present sense, defined the size of the primary recirculating cell. (Topham surmised that the wavering could serve as a barrier containing the oil released in a blowout, but the effect is much too weak to prevent the oil from spreading in the presence of wind, waves and currents).

The bottom layer in Topham's field test was slightly colder than the surface water ($\Delta\rho/\rho_w \approx 0.002$, where $\Delta\rho$ is the density difference between the surface and bottom layer and ρ_w is the mean density of water). The actual cell radius was about half the ocean depth of 60 m, and Topham measured the outward as well as the inward velocity outside 'the wavering'.

Fanneløp & Sjøen (1980) measured the radial surface flows from round bubble plumes at depths of 5 m and 10 m in a towing tank. The measurements at the smaller depth extended to $R/H = 2.1$ (where R is the radius of the plume and H the depth of the tank) or about four times the plume radius at the surface. A distinct change in the velocity profile is apparent at about $R/H = 1$, i.e. from a triangular to a peaky shape with the maximum velocity (horizontal component) well below the surface. It appeared that the outflow turned progressively downward further out, aided by a slight temperature stratification ($\Delta T = 2.5$ °C prior to the test and about 1.5 °C after a few hours of operation). Small pieces of paper placed in the plume region were carried outward to a distance of $R/H = 2$–2.5 whereupon they remained stationary for hours. This apparent limit of plume influence is of some interest as Goossens (1979) proposed (for isothermal flow) a region of influence in the range $R/H = 4$–7; the smaller value representing model tests and the larger full scale. Goossens presented a theoretical model as well as experiments in support of his findings, and he notes in particular the dependency of cell size on gas flow rate. Milgram & Burgess

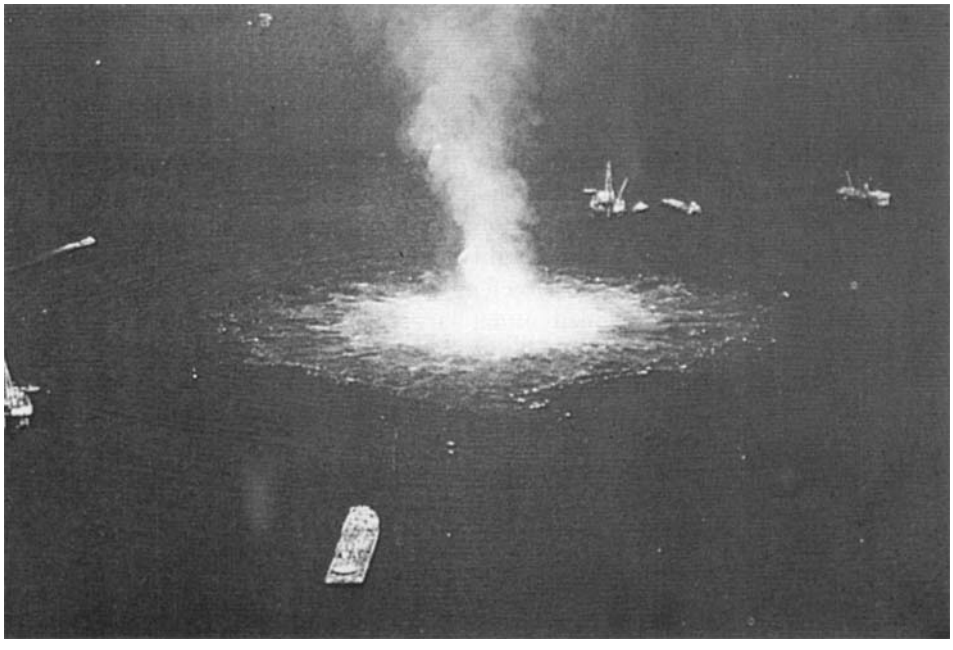

FIGURE 1. Offshore gas blowout, Fateh Field, Dubai (1977).
(Reproduced with permission from *Ocean Industry*, vol. 12, no. 19).

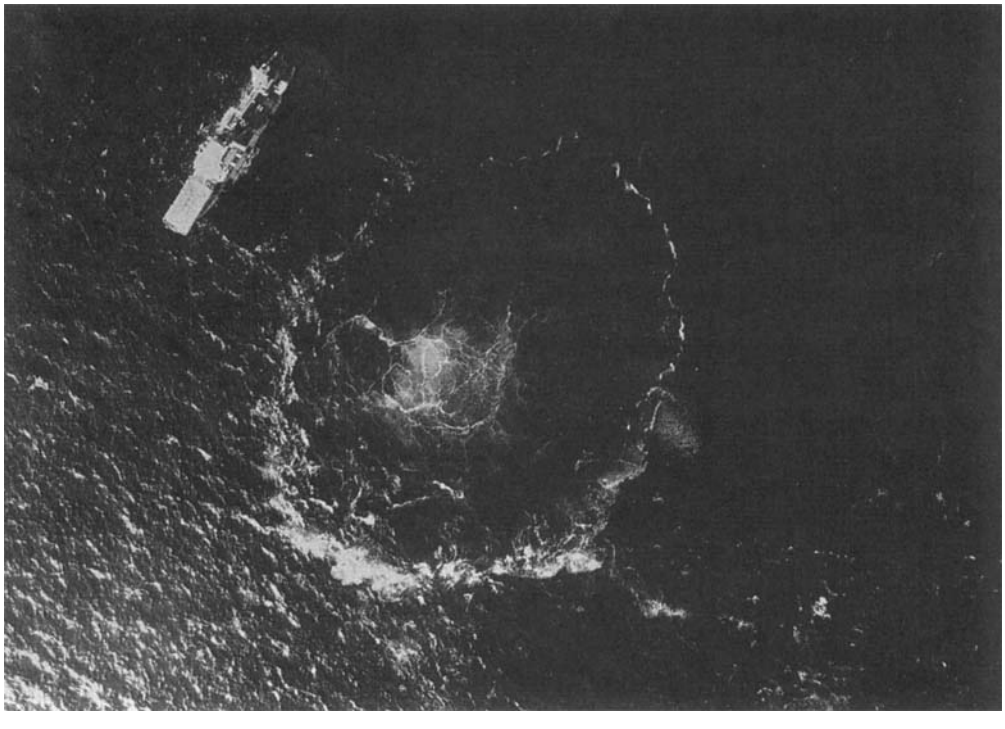

FIGURE 2. Blowout from shallow pocket, Haltenbanken, Norway 1985.
(Courtesy: Norsk Hydro Research Centre, Bergen.)

(1984) in their field experiment in a deep freshwater well (source depth about 50 m), verified and extended the data of Fanneløp & Sjøen but made no mention of a wavering. Spectacular photographs of real blowouts in offshore gas fields (Fateh, Dubai, 1977, figure 1, and Haltenbanken, Norway, 1985, figure 2), do indicate the presence of a ring domain which separates the foamy plume water, brought to the surface from below, from the undisturbed surface water outside. Stratification is likely to play a role in both situations. A rough estimate indicates a cell width (wavering diameter) about equal to the depth. For the Haltenbanken case, the estimate is quite reliable as the aerial photograph has an accurate lengthscale, but wave motion and currents introduce complications. In the Fateh case there are few disturbances, but the estimate can be made only with the help of 'scalable' objects nearby.

The conclusion to be drawn from this scattered information is that large-scale applications of bubble plumes in the ocean at depths typical of offshore fields, are likely to produce recirculating cells rather than an unlimited horizontal current. The surface flow outside is directed towards the primary cell but it is not known if this is a local counterflow or part of a secondary recirculating cell extending over the full depth.

3. Theoretical considerations

For the flow conditions of interest in actual applications, it is possible to derive simple (similarity) solutions for the plume flow which in turn can be used to estimate the horizontal current and the cell size. For depths in excess of 10–20 m, the bubble slip velocity will be small in comparison with the plume velocity, the 'zone of establishment' will be negligible in comparison with the total depth and the momentum flux carried by the turbulent fluctuations will be a small fraction of the mean-flow momentum. On assuming the plume parameters to be independent of depth, it becomes possible to obtain the general solution given in what follows. For the shallow depths of interest in laboratory investigations, the physical assumptions required for similarity can no longer be justified. It will be necessary to integrate the equations of motion numerically in each case. Additional empirical information on entrainment rate, on turbulent momentum flux, etc. is required to obtain a definite solution for each case. The full equations are given in the Appendix. Numerical solutions covering a wide range of parameters are included. It is clearly seen that the numerical solutions approach the similarity values a few metres above the source for plausible initial conditions. These results confirm those of Milgram (1983) for round bubble plumes.

3.1. *The plume from a line source*

In order to establish the initial depth and momentum of the surface current, it is necessary to determine the vertical fluxes of volume and momentum in the plume. It is reasonable to assume minimal losses in the impingement zone where the flow is deflected outwards along the water surface. Internal hydraulic jumps should not appear for non-buoyant or negatively buoyant discharges (Andreopoulos *et al.* 1986).

For gas releases at pressure depths much in excess of one atmosphere, the compressibility exerts a powerful influence on the plume characteristics. Gas expansion with decreasing depth increases the plume buoyancy. Investigations of axisymmetric plumes have shown that only an inner core of the plume contains bubbles. The ratio between the bubble core width and the (momentum) plume diameter (in effect the 'Schmidt number', here denoted λ) is an important plume

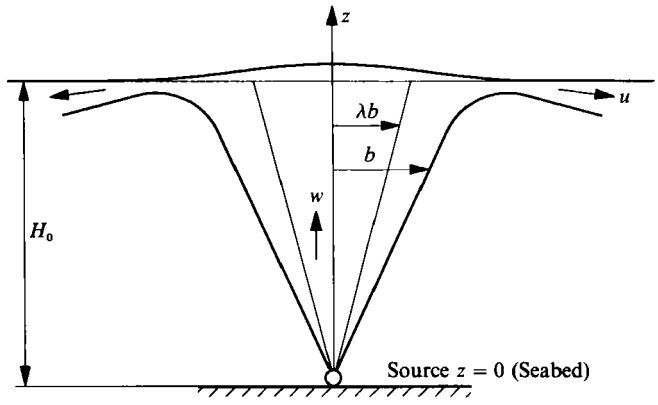

FIGURE 3. Plume geometry and flow variables.

parameter. For axisymmetric bubble plumes we have $\lambda = 0.6$–0.8, according to Fanneløp & Sjøen (1980) and Milgram (1983). Their experiments also show that the entrainment rate α depends on gas volume flow rate and perhaps also varies with distance from the source. Reliable data for λ and α for large-scale bubble plumes from line sources are not available. We will henceforth write the plume equations in a form which admits general similarity solutions. To this end the empirical coefficients α and λ will be taken as constants and the (small) bubble slip velocity ignored. But the compressibility is taken fully into account. This can be accomplished by following the approach used by Fanneløp & Sjøen for point sources. The gas expansion is assumed to follow a polytropic law:

$$\rho_g(z) = \rho_g(0)\left[\frac{p(z)}{p(0)}\right]^{1/n} \tag{1}$$

where z represents the distance from the source, ρ_g is the density of the gas and $p(z)$ is the pressure depth. Owing to gas expansion, the buoyancy flux is not constant, but the mass flux of gas is conserved. It is convenient to define the following non-dimensional parameters (see figure 3):

non-dimensional depth coordinate $$Z = \frac{z}{H_0 + 10\ \text{m}}; \tag{2a}$$

non-dimensional plume width $$B = \frac{b(z)}{\kappa\alpha(H_0 + 10\ \text{m})}; \tag{2b}$$

non-dimensional velocity $$W = \frac{w_m(z)}{M}; \tag{2c}$$

where $$M = \left(\frac{j\phi_0}{\gamma\kappa\alpha}\right)^{\frac{1}{3}}$$

includes the momentum amplification factor γ, as defined by Milgram (1983). It accounts for the momentum flux contribution associated with the turbulent fluctuations.

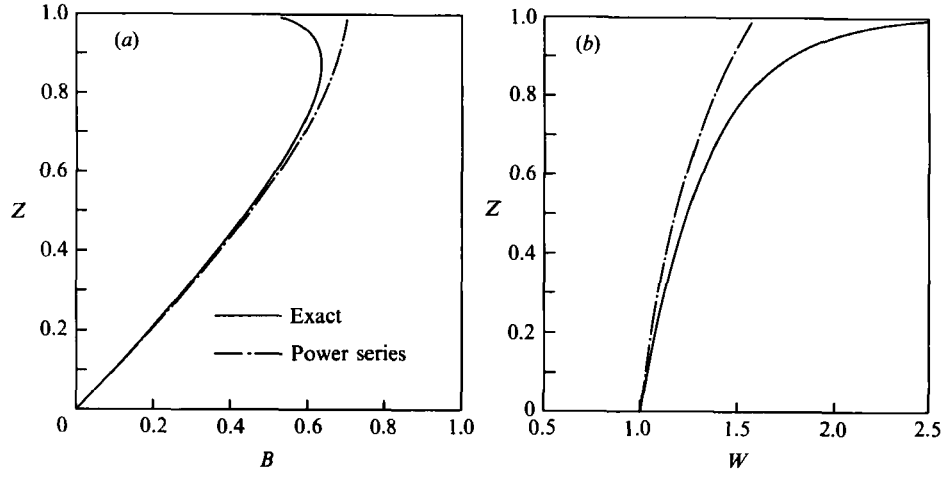

FIGURE 4. Comparison of power-series solutions for (*a*) B and (*b*) W with the exact solutions of the plume equations, $n = 1$.

In equation (2) the variable Z denotes the non-dimensional distance from the source, the source depth H_0 and distance are given in metres, and $\Delta z = 10$ m is (approximately) the water depth corresponding to the atmospheric pressure. The symbol B denotes the non-dimensional radius of the plume, the definition of the physical radius depends on the choice of profiles (tophat or Gaussian). The velocity $w(z)$ represents either the average (tophat) value or the Gaussian centreline value. The factors κ and j depend also on the choice of profiles. ϕ_0 specifies the buoyancy at the source; $\phi_0 = g\dot{V}_0$, where $\dot{V}_0$ is the gas volume flow rate. The plume parameters α and λ are considered to be known empirical constants. With these definitions, the integral plume equations for a line source can be written

$$\frac{\mathrm{d}}{\mathrm{d}Z}(BW) = W, \quad \frac{\mathrm{d}}{\mathrm{d}Z}(BW^2) = \frac{1}{W(1-Z)^{1/n}}. \tag{3a, b}$$

For slowly rising small bubbles and constant water temperature, the expansion is likely to be isothermal, i.e. $n = 1$. A singularity is apparent for $Z = 1$, but we note from the definition that Z can never attain this value.

A solution of these equations can be obtained in terms of a power series in Z. To fourth order this solution is

$$B(Z) = Z - \frac{1}{8n}Z^2 + \frac{1-32n}{480n^2}Z^3 - \frac{1920n^2+720n+60}{25040n^3}Z^4 + \ldots, \tag{4a}$$

$$W(Z) = 1 + \frac{1}{4n}Z + \frac{7+16n}{160n^2}Z^2 + \frac{640n^2+464n+58}{5760n^3}Z^3 + \ldots, \tag{4b}$$

where the leading term represents the 'constant-buoyancy' solution. The accuracy of the power-series solution is adequate to $Z \approx 0.5$ for W and perhaps to $Z \approx 0.8$ for B. A comparison with the exact solution is shown in figure 4 for the case $n = 1$.

It remains to specify the factors κ and j which depend on the choice of profiles.

For tophat profiles $\kappa = 1, \quad j = \frac{1}{2}\lambda;$ (5a, b)

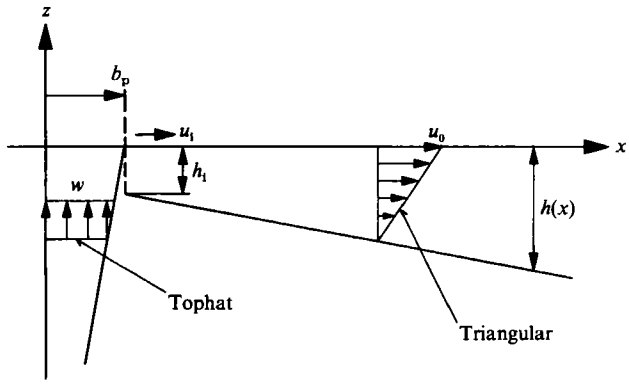

FIGURE 5. Flow model for the plume-generated horizontal current.

for Gaussian $$\kappa = \frac{2}{\pi^{\frac{1}{2}}}, \quad j = \left[\frac{2(\lambda^2+1)}{\pi}\right]^{\frac{1}{2}} \tag{6a, b}$$

The relevant Gaussian profiles are

$$w(x,z) = w_m(z)\,e^{-x^2/b_G^2}; \quad \rho_w - \rho(x,z) = [\rho_w - \rho(z)]\,e^{-x^2/\lambda^2 b_G^2} \tag{7a, b}$$

and the ratio $b_G/b = 2/\pi^{\frac{1}{2}}$ where b is the tophat value.

This simplified theory takes no account of bubble slip as noted. For small bubble plumes in the laboratory, the slip velocity (typical magnitude 0.3 m/s) is not small in comparison with the mean-flow velocity. Another complication is that an appreciable fraction of the kinetic energy appears as turbulent fluctuations, in particular for low gas flow rates and close to the source (Milgram 1983).

For larger plumes at greater depths, the solution given produces reasonable estimates of plume quantities, bearing in mind the uncertainties in the parameters α and λ. A review of existing data on bubble plumes with particular reference to the liquid volume flux, has been presented recently by Leitch & Baines (1989). (Owing to the diminutive scale of their 'weak plume' experiment, the new results are not relevant to our case.)

3.2. *The horizontal current and the cell size*

Only the unconfined case will be considered with the understanding that it is useful, as a first estimate, only for small current-to-depth ratios at large distances (in terms of plume widths) away from the plume. A schematic flow picture is given in figure 5. We will assume a triangular velocity distribution. This profile shape was used by Taylor and it comes close to the velocity profiles actually observed. We assume further that no momentum losses occur, as the upward-directed plume flow is deflected sideways. On denoting the surface current $u_0(x)$ and the current depth $h(x)$, we can derive, on the basis of a local balance of mass and momentum in the turning region, that

$$h(x) = 4\beta b_p\left[\frac{x}{b_p} + \frac{1-3\beta}{3\beta}\right], \tag{8}$$

$$u_0(x) = (\tfrac{4}{3}\beta)^{-\frac{1}{2}} w_p\left[\frac{x}{b_p} + \frac{1-3\beta}{3\beta}\right]^{-\frac{1}{2}}, \tag{9}$$

where β is the entrainment parameter and the index p denotes plume variables at the surface. The initial conditions have been applied at $x = b_p$ and one obtains (tophat plume solution)

$$u_{0i} = \tfrac{3}{2}w_p, \quad h_i = \tfrac{4}{3}b_p. \tag{10a, b}$$

The details of the analysis, for the analogous case of a round plume, are given in Fanneløp & Sjøen (1980).

Equation (8) and (9) are primarily useful in predicting the current and depth for values of h much smaller than the total depth as noted. Milgram (1983) has reviewed the existing data for the surface flows generated by round bubble plumes and finds good agreement between the simple theory and the measured surface speed. The entrainment parameter β is found to depend on gas flow rate. The values range from $\beta_G = 0.048$ to 0.15 (Gaussian profiles) for gas flow rates from 0.008 Nm^3/s to 0.364 Nm^3/s at source depths 5.5 m and 50 m. The dependence on gas flow rates of both entrainment parameters α and β implies that the cell size will depend on gas flow rate as well.

For the vertical plane jet, Jirka & Harleman (1979) argued that the spreading rate will be constant to give the half-width $b = 0.2s$, where s is the distance travelled from the line source, measured vertically in the jet half-plane and horizontally along the water surface. The breakdown of the jet flow is taken to occur where b equals the half-depth, i.e. for $s = 2.5H$ or $x = 1.5H$ horizontally from the jet source. They estimated, further, the turning zone to be of the order of $0.5H$ to give a cell length of about 2–$2.5H$. Jirka (1982) later proposed the value 0.15 for the spreading rate (Gaussian value). From Fanneløp & Sjøen's (1980) theory for the surface jet generated by a round bubble plume, the spreading rate is given approximately by

$$(\mathrm{d}/\mathrm{d}r)(h_G) = (2\pi^{-\frac{1}{2}})\beta_G.$$

This result is valid at large radii where the effects of the radial geometry is small. Milgram's (1983) review indicates a most likely value of $\beta_G = 0.061$ for the range of gas flow rates considered. The corresponding cell length for two-dimensional flows will be about twice the value estimated by Jirka & Harleman, and moreover dependent on gas flow rate. Further support for the low entrainment rate as well as the dependency on gas flow rate, will be found in the work of Goossens (1979). But this new estimate is uncertain because it is based on entrainment rates obtained in radial flows and because it assumes constant spreading rate in the surface current. Past measurements for round bubble plumes indicate gradual changes in the velocity profile, as noted by Milgram (1983).

The definition of cell length, based on the depth of the surface jet as proposed by Jirka & Harleman, cannot be related to simple observables. The field observations referred to earlier give better definitions; the stagnation line separating the primary cell from the counterflow outside can be easily detected. In the controlled environment of a laboratory, other phenomena are observed which can be used to define the cell length. The surface waves generated by the bubble plume have rough (turbulent) surfaces in the primary cell, but have smooth (reflecting) surfaces in the laminar flow outside, as shown in figure 6. A characteristic pattern of capillary waves can also be observed in the boundary region inward of the stagnation line. The latter is easily identified by eye, although it changes its shape and location continuously. In our experiment it was generally found within a region of extent about one half the depth. These visual observations can be verified by the more objective measures of velocity and mass flow within the cell. We note that the cell generated by the bubble

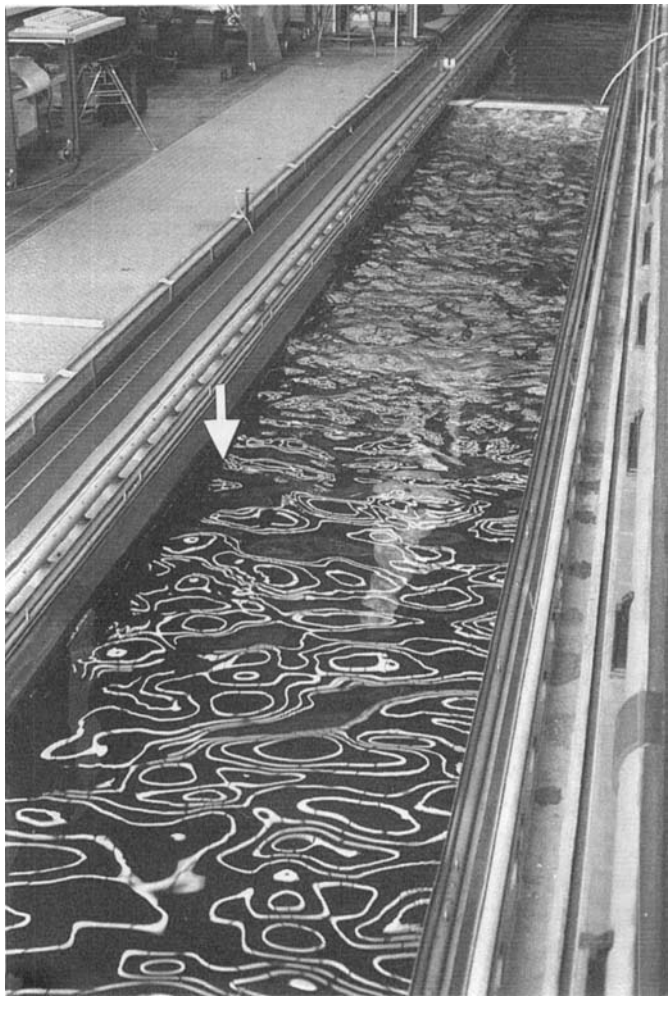

FIGURE 6. Surface appearance of flow in primary cell (rough) and outside (smooth) for the case of a plume-driven flow. (Cell boundary indicated by arrow.)

plume represents a closed stream surface, whereas the cell driven by the jet has net outflow. It appears that the secondary flow outside the primary cell is likely to be weaker in the case of plume flow. The cell limit for the jet flow is also conceptually less clear, except in the limit of vanishing initial jet volume flow rate. Jirka & Harleman did not measure the velocities in the recirculating flow region. Andreopoulos *et al.* give velocity data only for the upper half and for a limited length ($\max x/H = 1.66$) owing to problems with the LDA set-up. A complete mapping of the flow within the recirculating cell has not yet been published for either jet- or plume-driven flows. The measurements reported herein are in agreement with those of Andreopoulos *et al.* in the upper left quadrant of the cell, the only part measured by them. But by measuring the complete cell, a longer cell with a different flow structure is found in comparison with that proposed by previous investigators.

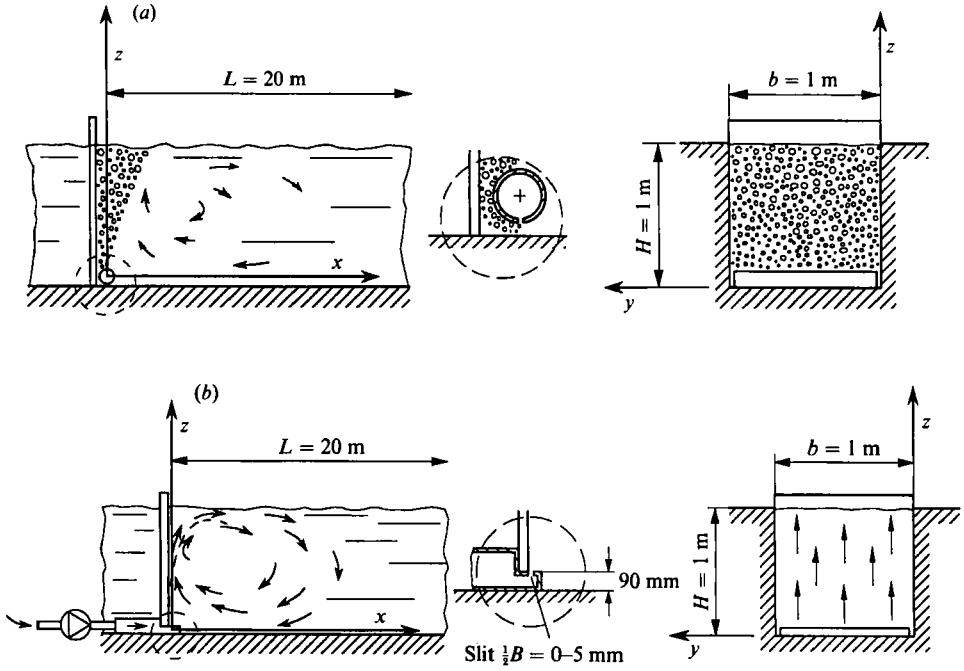

FIGURE 7. (*a*) Schematic of experimental set-up showing dividing wall and plume source. (*b*) Schematic of experimental set-up showing dividing wall and jet source.

4. Experimental facility and measurement technique

The experiments were conducted in the towing tank of the Institut für Flüssigkeitstechnik, ETH. The tank (which can also be operated as a flume) has principal dimensions of length, width and height of $L = 40$ m, $b = 1$ m and $H = 1$ m respectively. In the case of the bubble-plume experiments, the tank was closed at the far end. For the vertical plane-jet experiments the water level was kept constant by means of a weir. The tank has smooth concrete walls but no underwater windows. All visual observations had to be made from above, and although three-dimensional effects were easily recognized by eye, it was not possible to make a permanent record of all the phenomena observed. The tank and the associated water reservoir are contained inside the heated laboratory space, and the temperatures are therefore equal and essentially constant. Certain phenomena occurred which were due to the special geometry of the facility (i.e. long and narrow). But this geometry is typical for all towing tanks, and these phenomena may therefore be of general interest. One such phenomenon was a slow, periodic rotation of the plume crown of about $\pm 10°$, approximately once per minute. This instability was traced to asymmetric corner-flow separation in the source region. The plume flow has low momentum near the source and it can interact with the slow-moving return flow. Such an interaction is not likely to occur in the case of a jet. The instability was countered by introducing a dividing wall, figure 7 (*a*). For the additional experiments with a jet, the dividing wall was also used, figure 7 (*b*). It was, in most tests, installed at a distance of about 20 m from the endwall and weir. For comparison, the smaller channel used by Jirka & Harleman, had variable length, 3.7 m or 6.1 m, a constant width 0.305 m and water depth 0.3 m or 0.6 m. The channel used by Andreopoulos *et al.* had length of only 4.4 m and width 0.3 m. The water level was varied in the range 0.155–1.055 m.

These two channels and the general flow arrangement (free communication with an outside reservoir) were quite similar. Only Andreopoulos *et al.* present velocity measurements for non-buoyant discharge, the case of present interest. With the jet installed in the middle of the channel, the length-to-depth ratio, available for the formation of cells, was only 2.2 m/0.6 m = 3.7 in their experiments of present interest. This is much less than the typical value ($L/H = 20$) used by us. This difference is of concern as the primary cell observed in our experiments exceeded the available length in their channel.

To generate the line source, a steel pipe of inner diameter 26 mm and length equal to the channel width was anchored at the bottom by a heavy steel plate. Along a meridian line, 25 holes of diameter 0.8 mm were drilled at regular intervals of 37 mm. The hole diameter and the internal air pressure in the pipe ensured choked flow and therefore equal mass flow through each hole. The gas jets were directed downwards toward the anchor plate in most tests, to minimize the extent of the zone of establishment of the bubble plume. The pressure and rate of air supply were measured in the supply line with a commercial manometer and rotameter. Air was delivered from the available laboratory high-pressure air supply through an appropriate pressure-control system. Most of the early tests (for stability and three-dimensional effects) were run with a flow rate of 4.5 l/s, i.e. a source strength of $\dot{V} = 0.0045$ m^2/s (Hirschberg 1985; Brenner & Laghi 1987). With the dividing wall in place, the line source was located in the corner between the channel floor and the wall (figure 7*a*). The wall was made of Plexiglas and allowed us to observe the flow in the half plume; of particular interest were bubble size and distribution and the interaction between the bubbles and the flow instruments.

The plane vertical jet was generated as follows: a rectangular pressure vessel of width equal to the channel width, of length 0.6 m and height 0.09 m was placed on the bottom of the channel. Water was fed into the vessel under pressure and allowed to exit through a slit of constant width and length equal to the channel width, at the other end of the vessel. The dividing wall was mounted on top of the vessel flush with the inner edge of the slit (figure 7*b*). The slit half-width $\frac{1}{2}B_{\mathrm{Slit}}$ could be varied between 0 and 5 mm (half-jet) giving depth-to-slit-width ratios of 200 and over. The Reynolds numbers, based on jet exit conditions, $Re = B_{\mathrm{Slit}} u_0/\nu$, were mostly 8000–20000, i.e. considerably higher than for Andreopoulos *et al.* The higher exit velocities (typically 3 m/s) gave not only more reliable results for our velocity measurements, but also more realistic test conditions. The range of jet momentum was chosen to match that of the plume experiments, as determined immediately below the surface interaction zone, i.e. at depth 0.25 m.

The main instrument used to measure velocities was the impeller anemometer Mikro-Mini-Water (Make: Schiltknecht) which has small dimensions (propeller diameter 20 mm, external casing 25 mm) and which gives an electric signal suitable for electronic recording and data reduction. The low-inertia of the rotor ensured a frequency response sufficient for our purposes. The instrument was direction sensitive as manufactured, but had to be calibrated for both forward and reverse flow. The calibration curves were linear and show differences of about 15%. The minimum velocity for both directions was about 4 cm/s. (The velocities below this value reported herein represent averages of many readings, including negative and zero values.) Accurate calibration was facilitated by the tow wagon available. From earlier experiments with bubble plumes (Milgram 1983; Fanneløp & Sjøen 1980) it is known that only long-time-averaged measurements give repeatable results. The results presented here represent mostly 5 min. averages, with sampling rates of about

10 per s, the limit being given by the electronic memory available. To check the effects of the bubbly environment on the propeller anemometer, single bubbles were arranged to pass through the impeller in a flow of known speed (equal for both phases, water and gas). A single bubble of the size of interest was found to reduce the recorded speed momentarily by about 18% (average for a number of tests). The void fraction in the centre of the plume was for the cases of interest here less than 2%. It follows that the presence of bubbles is likely to cause errors at the most of the order of a few percent, which is satisfactory for the present purposes. The bubbles moved about 50% faster than the bulk water, and observations through the Plexiglas wall indicated that the passage of a bubble through the impeller was a rare event; of in all 20 photographs taken, not one showed this to occur.

A second instrument, an ultrasonic Doppler device, developed at the ETH, Institut für Biomedizin, was used to determine other plume variables of interest. For measurement of the bulk-water speed, this device was also calibrated by means of the tow wagon. (The instrument could give only magnitude, not direction.) With bubbles in close proximity, two speeds would be recorded, the near steady water velocity and a peak associated with the passing bubble. The device could be used therefore to determine both the inner plume core where bubbles are present, and the velocities of the bubbles as well as the bulk-water flow. For single bubbles of size 1–2 cm in quiescent water, the rise velocity was measured to be 0.25–0.29 m/s. The averaged difference between the maximum values (bubbles of all sizes) and the near steady (water) values in the plume, were somewhat smaller, about 0.15–0.25 m/s. But the data from the ultrasonic-Doppler device had to be evaluated from the pen-trace of the recorder, a somewhat subjective and less satisfactory procedure than the electronic data processing used for the impeller devices.

At the very low velocities encountered, qualitative information derived from wool tufts, colouring agents as well as surface wave patterns and movements provided additional and useful information on the existence and extent of recirculating regions and on the cell structure.

5. Results

5.1. *Measurements in the bubble plume*

Bubble plumes in water basins of depth 1 m or less are not really of interest for comparison with general plume theories; the 'non-similar' effects of finite-source volume, bubble slip, plume–surface interactions etc. are too strong. But for the present purposes it was important to ascertain through measurements that the flow had a typical plume character as it approached the surface interaction zone. The characteristics of interest were the velocity profile, density distribution and the momentum flux, as well as the values of α and λ to be inferred from the measurements. The turbulent amplification factor was not evaluated. Tekeli & Maxwell's (1978) measurements in round plumes of source depth equal to ours (1 m) show the flow momentum carried by the turbulent fluctuations to be less than 15% of that of the mean-flow momentum for a wide range of gas flow rates.

By Gaussian-profile fits to the data and by use of the equation of motion for the plume, we arrived at the following plume parameters:

$$\lambda = 0.85, \quad \alpha = 0.08.$$

These values seem reasonable in comparison with known values for round bubble plumes, but the entrainment rate, in particular, is likely to depend both on distance

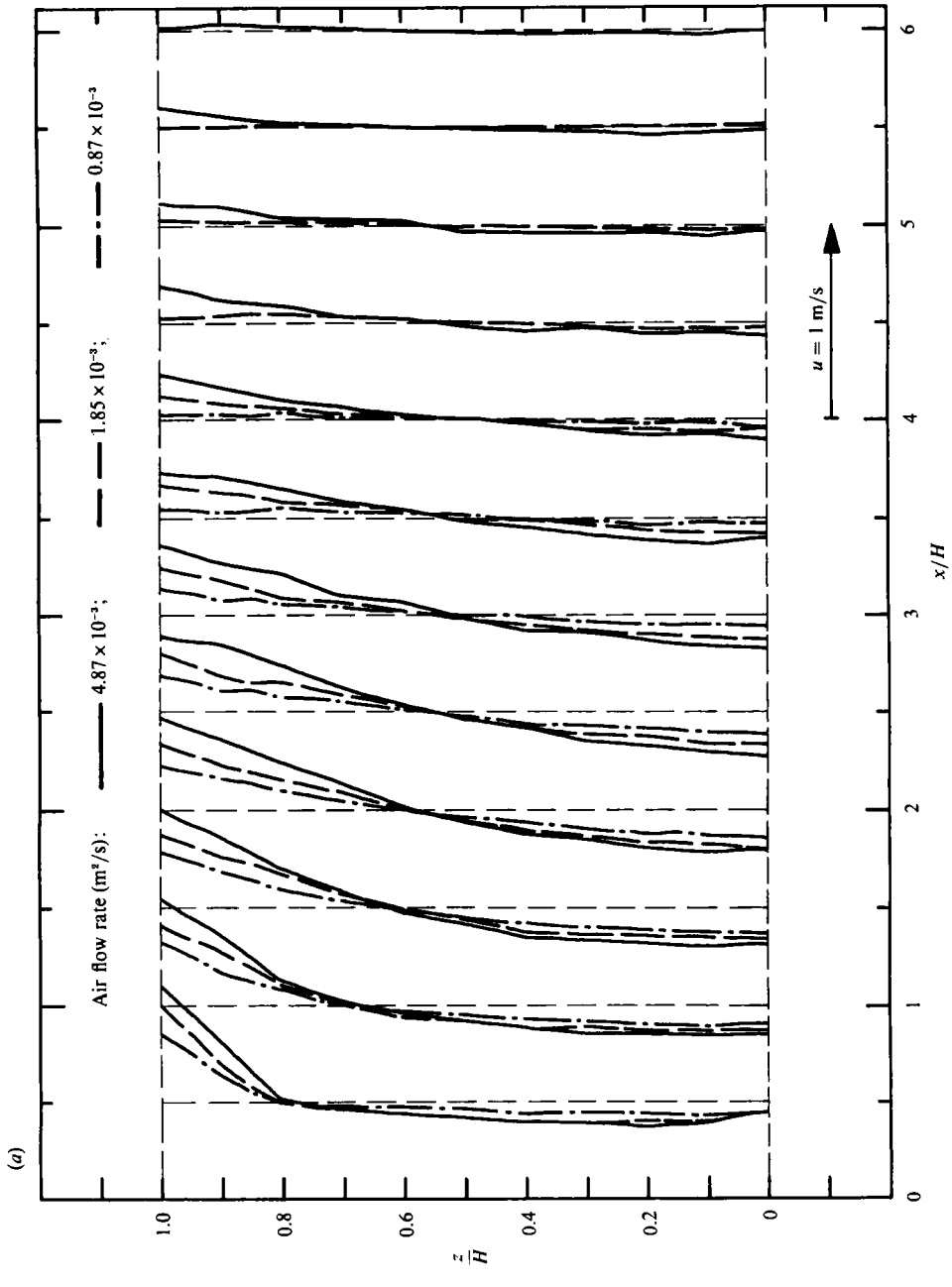
(a)
Air flow rate (m³/s):
4.87 × 10⁻³;
1.85 × 10⁻³;
0.87 × 10⁻³
u = 1 m/s
z/H
x/H
1.0
0.8
0.6
0.4
0.2
0
1
2
3
4
5
6

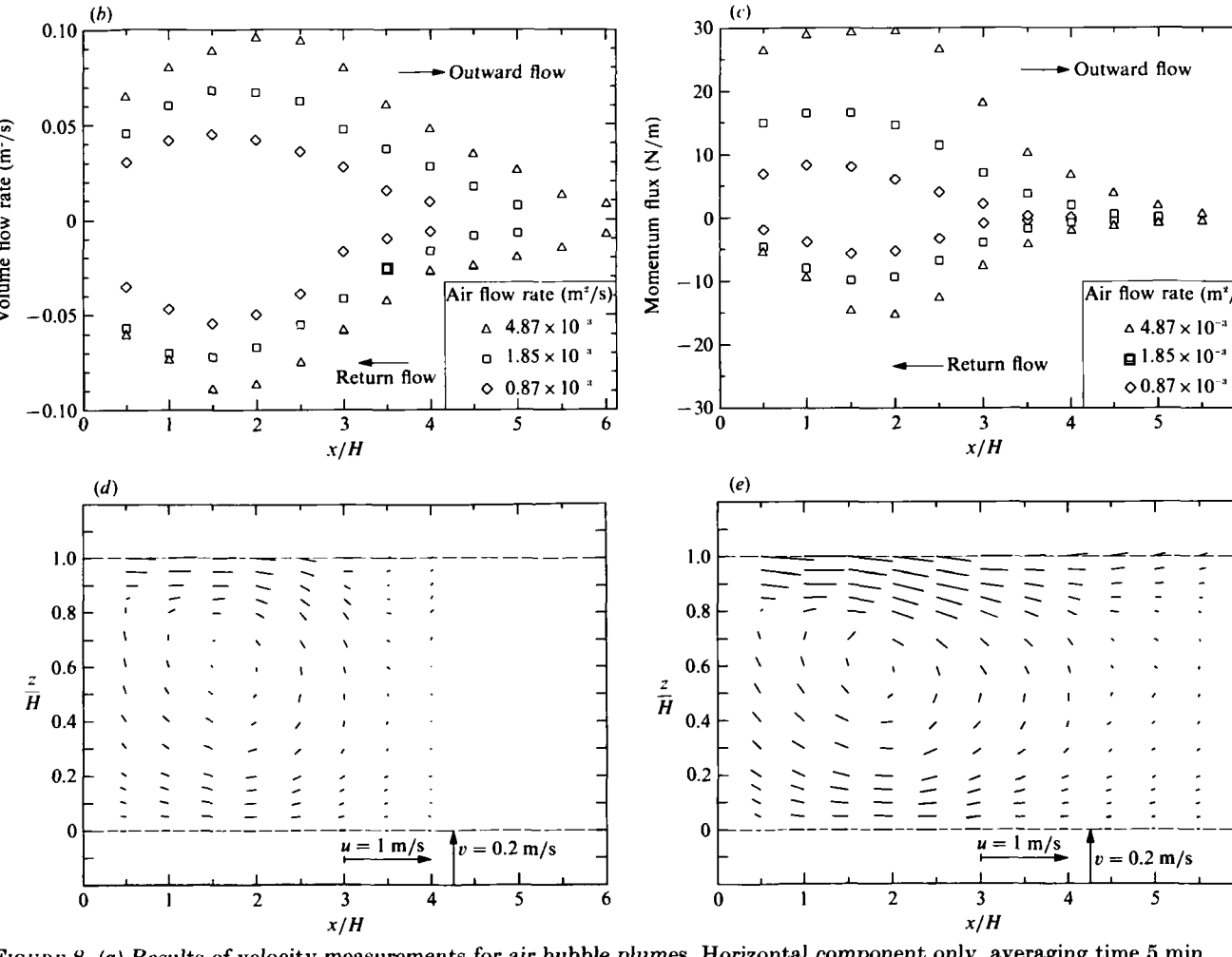

FIGURE 8. (*a*) Results of velocity measurements for air bubble plumes. Horizontal component only, averaging time 5 min. (*b*) Integrated volume flow rate for different plume air flow rates. (*c*) Integrated momentum fluxes (outward and inward) for various plume air flow rates. (*d*) Vector plot of flow velocity in recirculating cell for air flow rate 8.7×10^{-4} m²/s (Note scales). (*e*) Vector plot of flow velocity in recirculating cell for air flow rate 4.87×10^{-3} m²/s (Note scales).

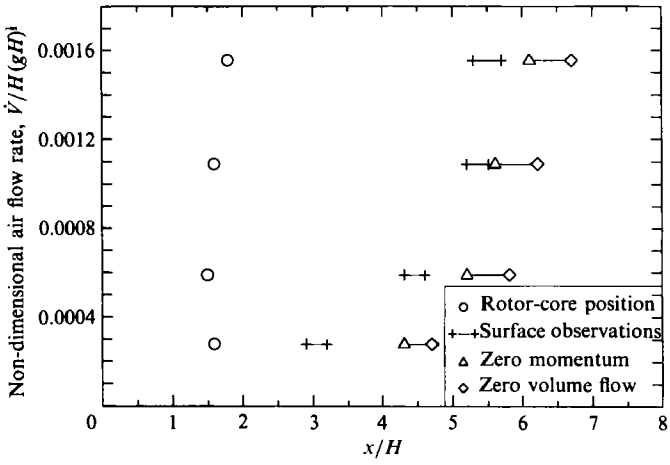

FIGURE 9. Cell length and rotor-core position as function of air flow rate.

from the source and on gas flow rate. The values given have been used primarily to estimate the plume momentum. In the case of the jet the momentum was determined from direct measurements with an impact probe. The flow character (profile and spreading rate) of the vertical jet flow outside the turning region agrees well with known data for the mean flow of plane turbulent jets (e.g. Jirka 1982). The boundary layer along the dividing wall did not appear to affect the results to any significant extent.

5.2. *Measurements in the plume-driven cell*

The velocity profiles along the centreline (horizontal component only) are illustrated in figure 8(*a*) for three volume flow rates in the range 8.7×10^{-4} to 4.8×10^{-3} m^2/s. A large number of cases without the dividing wall, but with and without flow straighteners to counter the instability in the source region, have been investigated as well. Results from these experiments will not be given; they are quite similar to those shown here, but exhibit stronger three-dimensional effects. All our tests show much longer cells than the estimates of cell length given in the literature. In figure 8(*a*) it is seen that the outward-moving current reaches the half-depth at $x/H \approx 5$, but the outward flow persists to almost $x/H \approx 7$ for the highest air flow rate investigated. This assessment is verified by the integrated volume flows in the outward and return directions (figure 8*b*) and finally by the momentum transport (figure 8*c*). From the measured velocity profiles of the horizontal component u, the vertical flow component v can be determined by mean of the continuity equation. Figures 8(*d*) and 8(*e*) show the vector plots $\boldsymbol{v} = (u, v)$ over the cell cross-section for the highest and lowest air flow rates. (The velocity components are scaled in the same proportion as the lengthscales.) The expected flow pictures of long recirculating cells emerge. The rotor cores are found quite close to the plume, in partial support of the 'short cell' suggested in earlier investigations. But the appearance of new 'secondary' and 'higher-order' cells seems most unlikely in view of figures 8(*d*) and 8(*e*). Results similar to figure 8(*a–e*) have been obtained for all flow cases investigated. Figure 9 shows the observed cell length as function of the non-dimensional flow rate $\dot{V}/H(gH)^{\frac{1}{2}}$ for all flow rates considered. The cell lengths based on surface observations (see figure 6) are seen to be somewhat shorter than those deduced from the velocity measurements. The variation of cell length with air-volume flow rate is about the same for all three criteria used, a weak dependence for the higher flow rates and a

rather substantial growth with flow rate at the lower end of the range. The position of the rotor core (as estimated from the velocity vector plots) is seen to be nearly independent of the volume flow rate.

5.3. *Measurements in the jet-driven cell*

Complete measurements have been made for three volume flow rates with an initial jet flow $\dot{V} = 5.7 \times 10^{-3}$, 8.1×10^{-3} and 1.17×10^{-2} m^2/s. The range matches roughly that for the plume flow (figure 8) in terms of momentum. Figure 10(*a*) shows the measured velocity profiles. In the region near the vertical jet these results are quite similar to those of Andreopoulos *et al.* (1986). As they took measurements at only four stations close to the jet ($x/H = 0.08$, 1.15 and 1.66), the determination of cell length becomes difficult at best. The cell length, as determined from figure 10(*a*), appears to be about $x/H = 5$; further corroboration comes from the volume flow measurements (figure 10*b*), from the integrated momentum transport (figure 10*c*), and from the vector plot of the total velocity (figure 10*d*). To obtain the vertical velocity v, the values of $\partial u/\partial x$ obtained from the measured velocities have been integrated from the bottom $y = 0$ to the free surface. The accumulated error is evident in the calculated flow directions; it is exaggerated through the distorted scales. The procedure used is more sensitive in the case of the jet-driven cell which has net throughflow, fluid is transported out of the cell. Only the case with the largest flow rate is included here (figure 10*d*) as this case has the best accuracy. In spite of the net outward transport, the limit of the cell was clearly visible to the eye. It was identified as the boundary between the turbulent rough-textured surface inside the cell and the smooth laminar surface outside (figure 11). The cell length for the jet-driven flow was independent of jet flow rate, in agreement with the similarity argument put forth by Jirka & Harleman (1979) although the flow profiles are clearly non-similar. But the actual length is twice the value they suggested. The cell was asymmetric with the rotor core quite close to the jet ($x/H = 1.5$) in all cases investigated (figure 12). (The difference in length between the surface observation and the interior flow measurements can be related to Jirka & Harleman's 'turning radius', which they estimated as $R = 0.5H$.) A localized outflow from the cell, near the surface, near the bottom or in between, could not be detected. It appears that the excess mass flow produced by the jet was distributed over the whole end surface and not, as expected, localized near the free surface.

5.4. *Measurements outside the cell*

The effect of the distant endwall on the size and the flow structure in the plume-driven cell, was investigated by inserting a 'false' endwall at various distances (from 8 to 20 m) from the source. No effect was observed. In the jet-driven case the distance between the injection slit and the weir was also 20 m in most cases. To ensure independence of channel length, a number of tests were conducted with much longer and somewhat shorter distances, with no observable change in cell size or character. The region outside the cell appeared in all cases to be laminar. This could be checked by dye injection. We were able to follow individual dye streaks over the full length of the channel outside the cell. From the dye movement, the extent of the cell could again be verified, but individual dye traces often indicated a distorted cell form in comparison with the time-averaged results. But most surprising was the observed flow structure in the laminar region. Dye streaks injected 3 cm above the bottom and 3 cm below the surface both moved towards the cell end. Here the flow turned vertical, converged towards middepth and flowed away from the cell at this level. This two-layer flow was observed not only for the plume but also for the jet over the

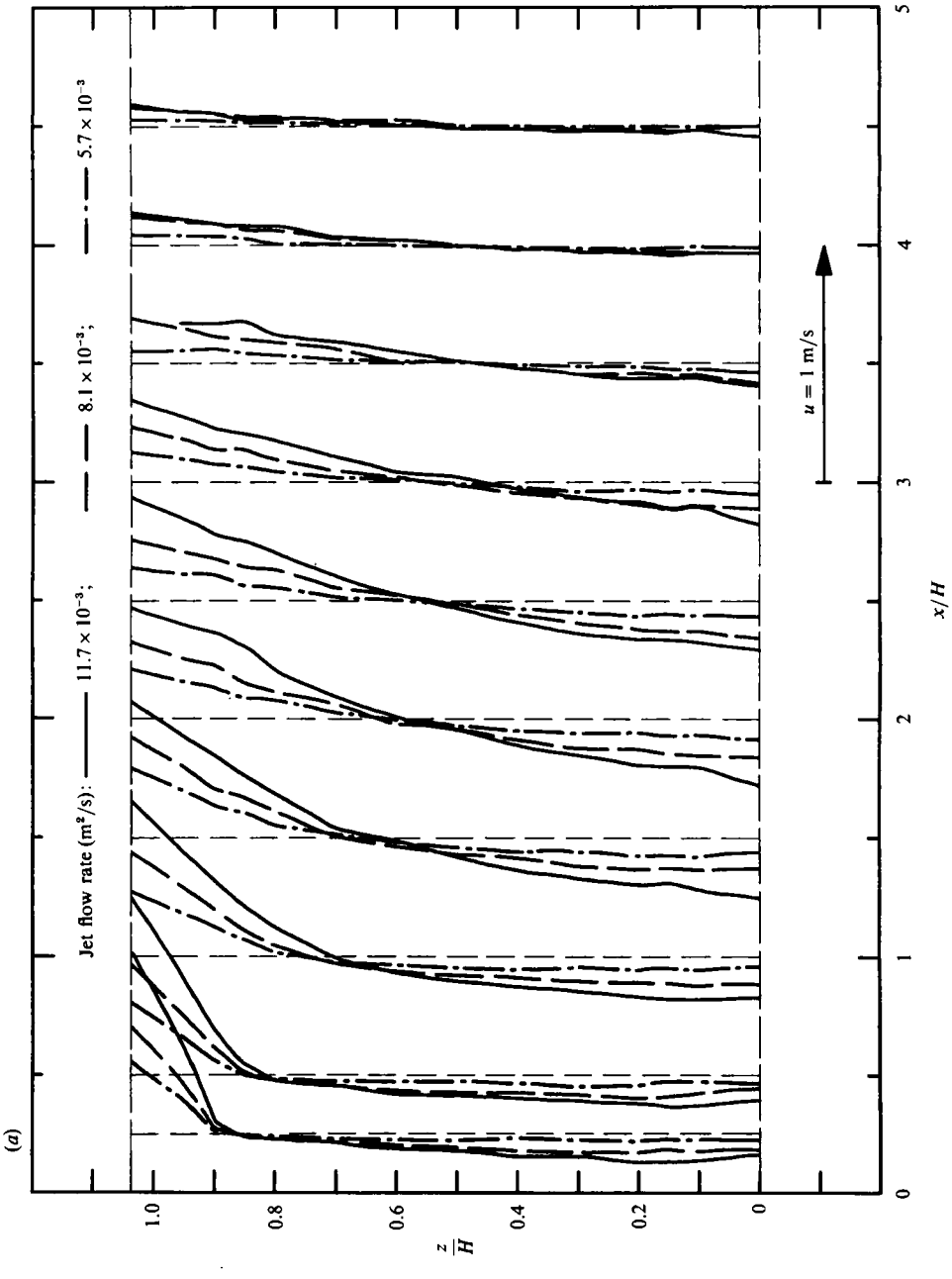
(a)
Jet flow rate (m²/s): —— 11.7 × 10⁻³; — — 8.1 × 10⁻³; —·— 5.7 × 10⁻³
u = 1 m/s
z/H
x/H
1.0
0.8
0.6
0.4
0.2
0
0
1
2
3
4
5

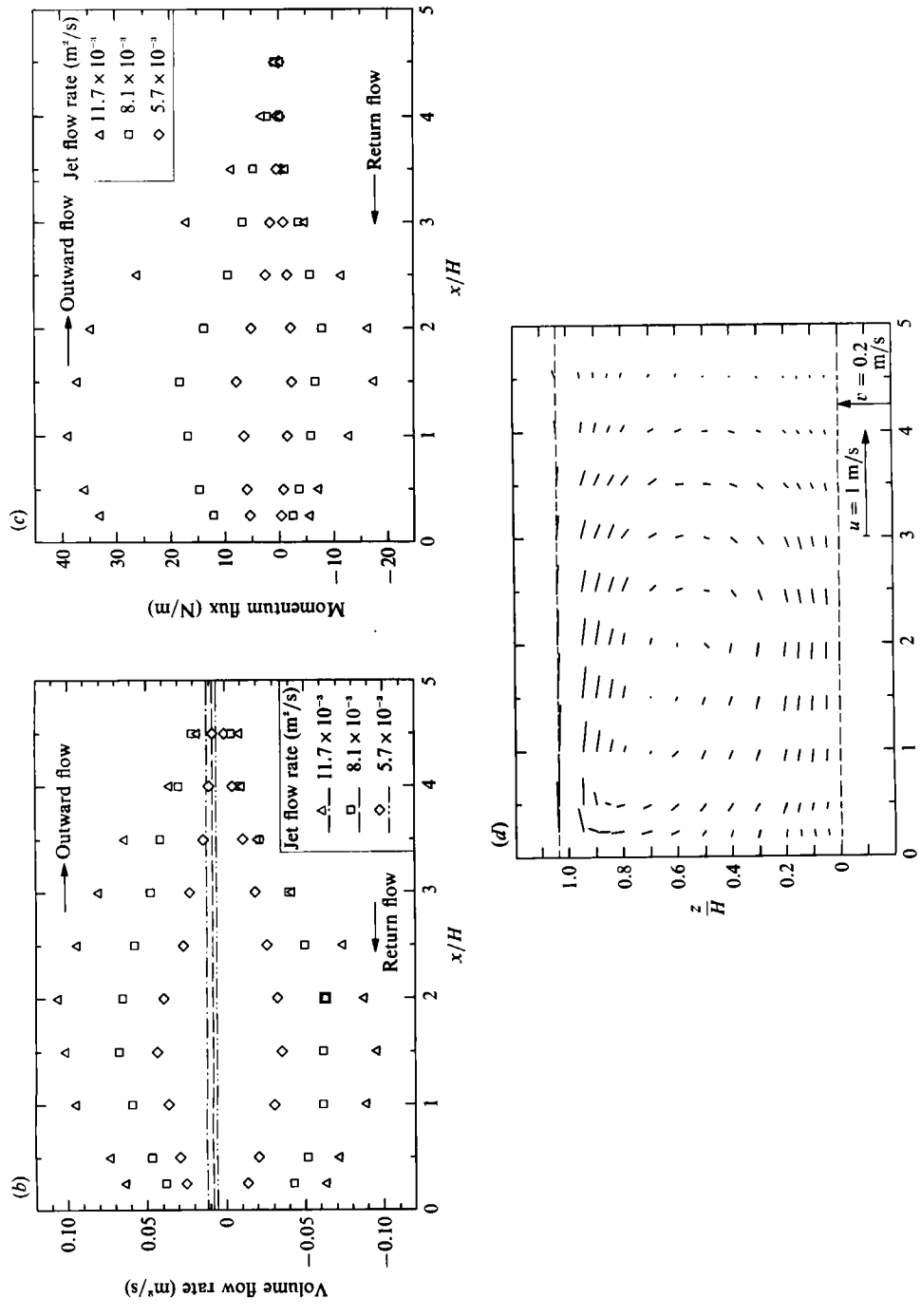

FIGURE 10. (*a*) Velocity measurements for different initial jet flow rates, $H/B_{\text{Slit}} = 294$. (*b*) Integrated volume flow rates for jet-driven cell. (*c*) Integrated momentum fluxes for jet-driven cell. (*d*) Vector plot of flow velocity in jet-driven cell. (Jet initial volume flow rate, $\dot{V} = 11.7 \times 10^{-3}$ m²/s, $H/B_{\text{Slit}} = 294$.)

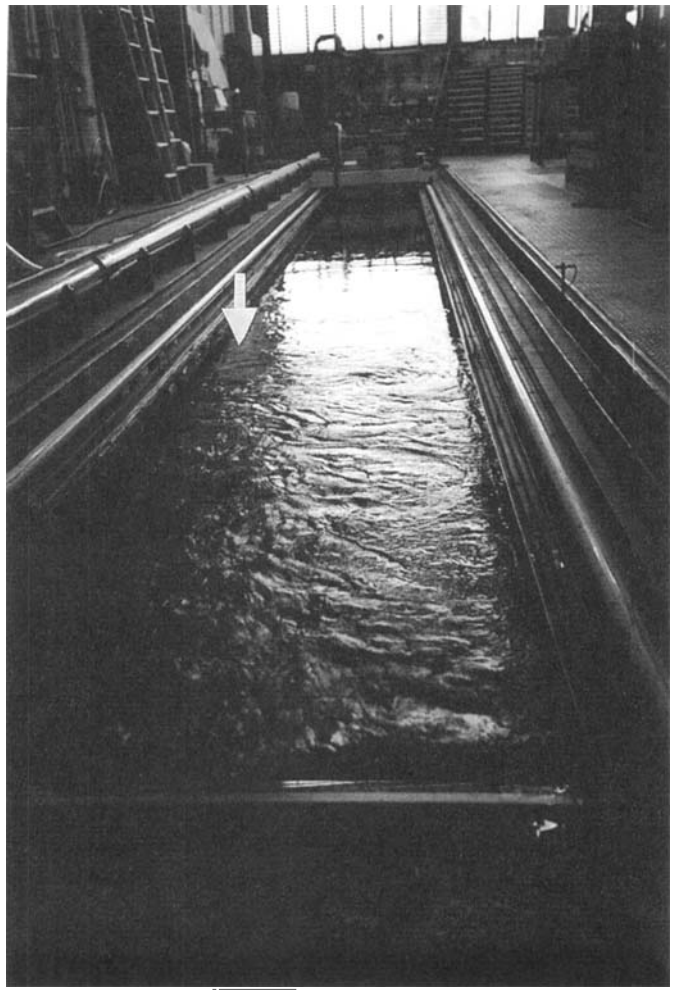

FIGURE 11. Surface appearance of flow in primary cell (rough) and outside (smooth) for the case of a jet-driven flow (cell boundary indicated by arrow).

full length of the laminar region (except close to the weir). The timed flow velocity, determined only for the plume, was typically about 0.3 cm/s in the laminar region, much below the threshold for our anemometer, but significantly higher than the 'disturbance velocities' in the channel. (One hour after the completion of a towing test, the residual velocities have been measured to be 0.1 cm/s or less, T. Staubli, personal communication.) The observed flow with sustained velocities substantially higher must be driven by the plume or jet or a plume- or jet-related phenomenon.

The measurements of temperature prior to the tests showed near constant values at all stations and all depths (for the plume experiments in winter 13.4 °C $\pm$ 0.2 °C). Only in a very thin boundary layer (of the order of 10^{-2} m) near the surface and near the bottom were higher values observed (14.7 °C, resp. 12.9 °C). The temperature difference of 1.8 °C is sufficient to be of interest, but the water mass within these boundary layers was negligible in comparison with the mass transport observed. Temperature measurements with the plume turned on showed no significant changes outside the surface region. Near the surface irregular disturbances produced by bubbles and plume turbulence affected the measurements. To check on long-term

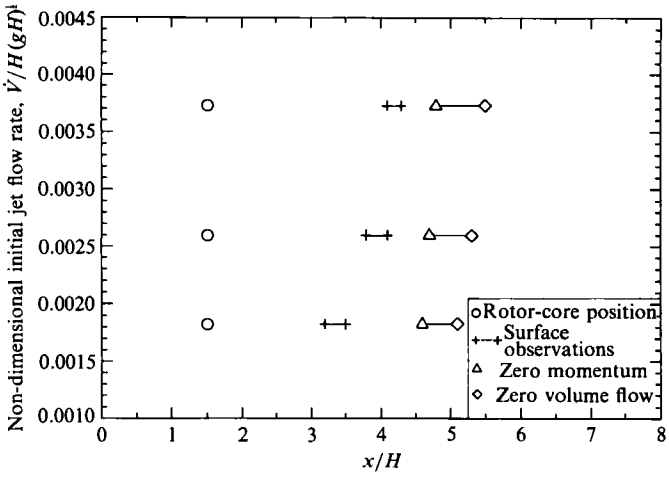

FIGURE 12. Cell length and rotor-core position as function of initial jet volume flow rate ($H/B_{\text{slit}} = 294$).

effects, the plume was left running for more than 16 h in one case, with no measurable changes in temperature or flow conditions.

One question which cannot yet be answered is whether or not the observed two-layer flow structure is a general phenomenon or facility specific. A second and perhaps more interesting question is whether the movements present in our channel prevented the formation of secondary and higher-order cells. To answer these questions we plan to modify our facility to allow underwater observations and measurements. We also plan to vary the width–depth ratio of the flow investigated. We note that the second-order cells extending over the full depth and of opposite rotation to the primary cell, suggested in earlier investigations, have never really been observed. The observation that the primary cell is much longer than assumed up to now, with little motion at the downstream end, makes the existence of secondary cell seem less likely.

5.5. *Entrainment rates in the recirculating region*

Based on the flow measurements presented in §§5.2 and 5.3, it is possible also to evaluate the entrainment parameter β appearing in (8) and (9). An evaluation based on the surface velocity produces large scatter. Owing to the presence of surface waves and the finite size of our measurement device, we could not measure the actual surface velocity, $u_0(x)$ given by (9), and extrapolation is required to obtain this result. More consistent values of the entrainment parameter can be obtained based on the depth $h(x)$ of the current. The relevant data are given in figures 8(*a*) (plume) and 10(*a*) (jet). The results, valid for triangular velocity profiles, are shown in figures 13(*a*) (plume) and 13(*b*) (jet). The measured depths have been normalized by the plume dimension b_p, established from the measured horizontal volume and momentum fluxes at $x/H = 1$, i.e. outside the turning region for both jet and plume. For the three volume flow rates considered, the values obtained for the plume or jet width were not much different, as expected. Averaged values have been used to present the data; i.e. $(b_p)_{av} = 0.244$ m (plume) and $(b_p)_{av} = 0.208$ m (jet). The lines in figures 13(*a*) and 13(*b*), show the predicted spreading rates of the horizontal jet for fixed values of the entrainment parameter, i.e. $\beta = 0.02$, 0.04 and 0.06. Only the slopes of these lines are of interest. The intersection point is somewhat arbitrary, but

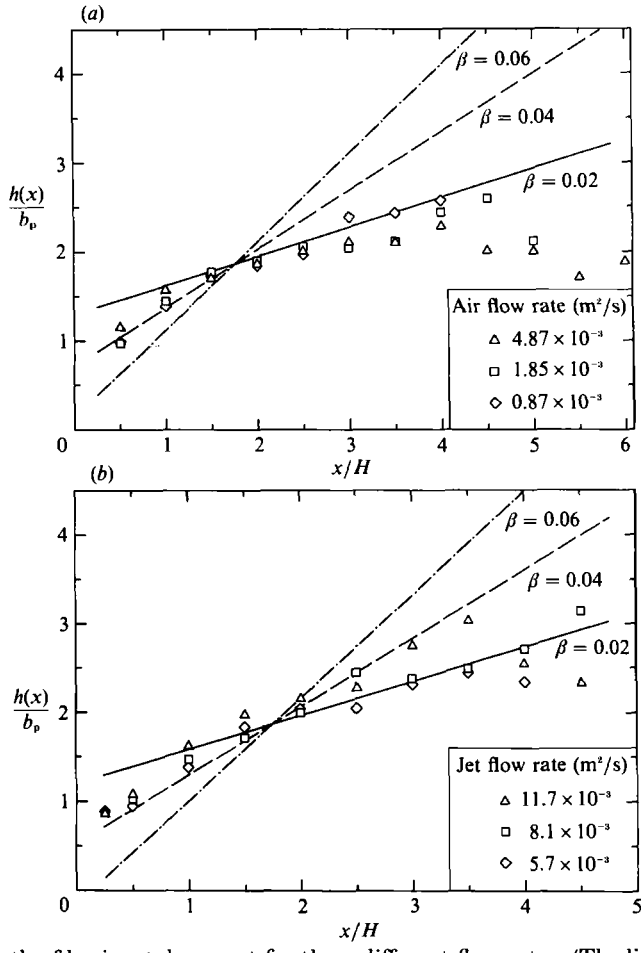

FIGURE 13. Depth of horizontal current for three different flow rates. (The lines indicate predicted rate of growth for fixed values of the entrainment parameter β.) (*a*) Plume-driven cell. (*b*) Jet-driven cell.

it indicates roughly where a reduced rate of growth characterizing the outer region is observed. From figure 13(*a*) we see that the value $\beta = 0.02$ gives the best overall fit to the plume data. For the jet (figure 13*b*) a slightly higher value seems justified, i.e. $\beta = 0.03$. To check on this result, we have evaluated the data for non-buoyant jets presented by Andreopoulos *et al.* (1986, Figure 21), and find here the value $\beta \approx 0.03$ also, again assuming triangular profiles. The corresponding Gaussian spreading rate would be about 0.065, i.e. one third the value used by Jirka & Harleman to estimate the cell length. Based on the experimental value of the spreading rate in the horizontal jet, Jirka & Harleman's estimate gives a cell length $x/H \approx 4.5$–5, i.e. about the value actually observed. But this is perhaps fortuitous, as the flow changes its character in the outer part of the cell.

6. Discussion

The interest in recirculating cells, their size and flow characteristics, is not merely academic. The efficiency of jets and plumes in the technical applications of present

interest depends on how far the surface jet reaches and on how much fluid it entrains prior to breakdown. A short cell indicates poor performance for most applications.

The present investigation is concerned only with non-buoyant flows which, not unexpectedly, produce recirculating cells. The information obtained for plume-driven flows is not in conflict with the meagre information available in the literature. The long cells observed are consistent with the increase in wave height starting at a distance from the plume baseline equal to six times the depth, as reported by Bulson (1963). The dependence of cell length on gas flow rate is in accord with previous observations by Goossens (1979), Fanneløp & Sjøen (1980) and Milgram & Burgess (1984). The turbulence generated by the rising bubbles in the plume is the likely cause. For the jet flow, where this effect is not present, the cell length does not depend on volume flow rate, although the surface jet is not self-similar.

Our results for the jet-driven flows are to some extent in conflict with observations and estimates previously reported, and we will herein primarily discuss these differences although the initial intent of our investigation was to focus on plume flow. We will consider first the problem of cell length and then the flow external to the primary cell.

Jirka & Harleman (1979) include references to several investigations in support of their estimate of a short cell. For the most part, these investigations differ in set-up and flow geometry from that of present interest. Most relevant is the experiment of Iamandi & Rouse (1969). But the channel length used was only four times the depth or less, i.e. significantly below the length of the primary cell found in our investigation. We conclude that the cell length observed was forced by the endwall, much like the case of Andreopoulos *et al.* (1986). G. H. Jirka (personal communication) has informed us that the observations on which the short-cell estimate was based represent slightly buoyant flows and that there is strong reason to believe that the buoyant inflow acts to diminish the available ambient depth and hence effectively shortens the cell. He also cites available information which predicts longer cells (Abramovich 1963).

W. Rodi (personal communication) points out that our vertical jet is really a wall jet which is known to have a much reduced turbulence level relative to a regular jet (Launder & Rodi 1983). This could be a contributing cause to the longer cell through reduced entrainment. Our set-up did not permit removal of the dividing wall, except for the plume experiment. Apart from the instability observed (see §4), there was no significant change in flow pattern or in cell length with the dividing wall removed (Hirschberg 1985). In the jet experiment we tried to cover the first part of the free surface with a deflector plate of length equal to the depth, in effect doubling the length of the wall-jet region. No significant change in the length of the jet-driven cell was observed, but the remaining (uncovered) free surface in the cell was noticeably smoother than before. The purpose of this test was to check on the possible momentum losses associated with jet deflection against a free surface (Hüsler 1988).

Rodi also points to the importance of the geometry of the channel cross-section and of the friction on the sidewalls which affects the return flow. For a purely two-dimensional flow, McGuirk & Rodi (1977) predicted a cell length of $4H$–$5H$ using the TEACH elliptic equation solver and the $k-\epsilon$ turbulence model, i.e. about the same length as found in the experiment. The predicted location of the rotor core also agrees with our experiments.

In view of these comments and the new information obtained it appears that the long cells reported herein represent an acceptable correction to the results previously

published for the non-buoyant case. (Many of the references cited, are concerned primarily with buoyant flows.)

The problem associated with the external flow, of whether or not secondary (and higher-order) cells exist, is more difficult to answer. An antisymmetric flow pattern with cells of comparable size, as in the all-laminar case, is not to be expected. The primary cell is clearly turbulent, but the second cell would already be laminar except in the mixing region shared with the primary cell. A flow which in character and direction agrees with the very plausible model suggested by Jirka & Harleman (1979) has been observed only locally in the surface region close to the primary cell (stagnation line or 'wave ring'). We exclude here observations from channels where the cell length is determined by the endwall.

No measurements exist of velocity and flow direction that fully confirm the Jirka–Harleman model with its succession of counter-rotating cells. Implicit in this model is the assumption that the shear, in the boundary region between the cells, represents the driving force. But at large distances from the baseline the jet acts as a volume source and produces an outward-directed velocity not necessarily small in comparison with the velocities likely to be found outside the primary cell. The model makes no provision for this source-flow effect associated with a finite-volume flow rate.

In the present experiment (§5.4) we can identify three forces: the shear force just discussed: the buoyancy force associated with temperature boundary layers near the free surface and the channel floor: and the pressure force associated with the jet considered purely as a volume source. From our velocity measurements we have evaluated the shear stress caused by gradients in the mean flow at the downstream end of the primary cell. To estimate the buoyancy force, we have used the temperature jump ($\Delta T = 0.9°$) near the surface prior to the test. This should give a high estimate. (Temperature measurements during a run were affected by disturbances generated in the jet-turning region, and are considered less reliable than the data obtained prior to a run.) The buoyancy and shear forces were found to be orders of magnitude smaller than the pressure force associated with the source, which we estimated to be about 1 N. (For the shear force our estimate gives 10^{-2} N, accounting only for the turbulent shear associated with the mean flow. For the (stabilizing) buoyancy force our estimate gives 10^{-3} N.) The mass to be set in motion by the shear force against the buoyancy force amounts to 3000–5000 kg for a cell length of 3–5 m. The source produces a pressure gradient which at large distances from the primary cell determines the unidirectional two-dimensional flow observed near the weir. But other mechanisms, yet to be identified, could exist as well inasmuch as the plume (no source term) and the jet produced the same flow pattern exterior to the primary cell, and not too close to the weir. We do not know if these results are general or particular to our channel or experimental set-up. But in view of the near-vanishing shear stress at the cell boundary, the flow model suggested by Jirka–Harleman appears not to be verified.

It is a pleasure to acknowledge helpful advice from a number of colleagues who have seen and commented on the experiment or on the data obtained. We thank Professors J. Imberger, G. H. Jirka, N. Kotsovinos and W. Rodi for their time and interest. We also thank Drs F. G. Nielsen and K. Herfjord of the Norsk Hydro Research Centre, Bergen, for technical information on offshore topics.

Appendix. Effects of bubble slip and finite gas fraction

In the highly turbulent environment of the established plume flow, most bubbles are small (typical diameter 1 cm). The rise velocity for a single bubble of this size in quiescent water is about 0.3 m/s, and it is usual in the theory of bubble plumes to postulate an excess velocity of the gas flow relative to the bubble mean flow of this amount. (For further discussion and justification of this 'slip velocity' see Fanneløp & Sjøen 1980 or Milgram 1983.)

The mean plume velocity, above a *point source*, generally decreases with the one-third power of distance, in the absence of gas expansion. The effects of a constant slip velocity, $w_s = 0.3$–0.4 m/s represent, for small gas flow rates, a non-negligible contribution to plume dynamics (for a detailed investigation, see Milgram 1983). The mean plume velocity above a *line source* is nearly constant (when gas expansion is excluded) and bubble slip would therefore appear to be less important in this case. This justifies the use of the similarity solution discussed in §3.1. In further support of this approximate but simple and accurate solution, we will here solve the full non-similar equations including slip (w_s), turbulent amplification of momentum (γ) and gas expansion. A detailed account is given in what follows, as it appears that a complete solution to the problem of line bubble plumes has not been published. The present approach is analogous to Milgram (1983).

On defining the local gas fraction ϵ by

$$\epsilon = \frac{\rho_\ell - \rho(x,z)}{\rho_\ell - \rho_g(z)}, \tag{A 1}$$

the fluxes of gas (subscript g) and liquid (subscript ℓ) mass and momentum can be expressed (for a unit length in the direction of the line source) by the following integrals

$$\dot{m}_g = 2\int_0^\infty \rho_g(z)\,[w_\ell(x,z) + w_s]\,\epsilon\,\mathrm{d}x, \tag{A 2}$$

$$\dot{m}_\ell(z) = 2\int_0^\infty \rho_\ell\, w_\ell(x,z)\,(1-\epsilon)\,\mathrm{d}x, \tag{A 3}$$

$$I(z) = 2\int_0^\infty \gamma\{\rho_\ell\, w_\ell^2(x,z)\,(1-\epsilon) + \epsilon\rho_g(z)\,[w_\ell(x,z) + w_s^2]\}\,\mathrm{d}x. \tag{A 4}$$

The factor γ, which represents the ratio of total to mean momentum flux, will be greater than unity and is considered to be known and independent of z. We note that $\dot{m}_g$ = constant in the absence of changes of phase (hydrate formation, boiling etc.). To facilitate the integrations, Gaussian profiles will be assumed. All relevant experimental information indicates profiles of this form:

$$w_\ell(x,z) = w_m(z)\,\mathrm{e}^{-x^2/b^2}, \tag{A 5}$$

$$\epsilon(x,z) = \epsilon_m(z)\,\mathrm{e}^{-x^2/\lambda^2 b^2}, \tag{A 6}$$

where

$$\epsilon_m(z) \approx \frac{\rho_\ell - \rho_m(z)}{\rho_\ell}$$

(The approximation $\rho_\ell - \rho_g(z) \approx \rho_\ell$ is accurate at all practical depths.)

On carrying out the integration (A 2) leads to the useful relations

$$\rho_{\mathrm{m}}(z) = \rho_\ell - \frac{\dot{m}_{\mathrm{g}}}{\rho_{\mathrm{G}}\,\pi^{\frac{1}{2}}\lambda b\left[\dfrac{w_{\mathrm{m}}}{(\lambda^2+1)^{\frac{1}{2}}}+w_{\mathrm{s}}\right]}, \tag{A 7}$$

$$b(z) = \frac{\dot{m}_{\mathrm{g}}}{\rho_{\mathrm{G}}(\rho_\ell-\rho_{\mathrm{m}})\,\pi^{\frac{1}{2}}\lambda\left[\dfrac{w_{\mathrm{m}}}{(\lambda^2+1)^{\frac{1}{2}}}+w_{\mathrm{s}}\right]}, \tag{A 8}$$

where $\rho_{\mathrm{G}} = \rho_{\mathrm{g}}/\rho_\ell$, and b, $w_{\mathrm{m}}, \rho_{\mathrm{m}}$ and ρ_{g} are functions of z.

The gas expansion will be considered isothermal, i.e. the gas density is proportional to hydrostatic pressure:

$$\rho_{\mathrm{G}}(z) = \rho_{\mathrm{G}}(H_{\mathrm{A}})\frac{H-z}{H_{\mathrm{A}}}, \tag{A 9}$$

where H_{A} is the atmospheric pressure head, about 10 m of water, and $H = H_{\mathrm{G}}+H_{\mathrm{A}}$ where H_{G} is the geometric source depth.

In addition to the invariance of gas flow rate,

$$\frac{\mathrm{d}\dot{m}_{\mathrm{g}}}{\mathrm{d}z} = 0, \tag{A 10}$$

the rate of change of momentum can be expressed in terms of buoyancy force

$$\frac{\mathrm{d}I}{\mathrm{d}z} = 2\int_0^\infty \epsilon(x,z)\,\rho_\ell[1-\rho_{\mathrm{G}}(z)]\,g\,\mathrm{d}x \tag{A 11}$$

where $\epsilon(x,z)$ is given by (A 6).

To close the system of equation, the turbulent entrainment is modelled as

$$\frac{\mathrm{d}\dot{m}_\ell}{\mathrm{d}z} = 2\alpha\rho_\ell\, w_{\mathrm{m}}(z). \tag{A 12}$$

To solve this system of equations by numerical integration, we introduce new parameters

$$\phi(z) = w_{\mathrm{m}}(z), \quad \Psi(z) = w_{\mathrm{m}}(z)\,b(z). \tag{A 13a, b}$$

After considerable algebraic manipulations, the equations to be integrated can be expressed as

$$C_1\frac{\mathrm{d}\psi}{\mathrm{d}z}+C_2\frac{\mathrm{d}\phi}{\mathrm{d}z} = C_3, \quad C_4\frac{\mathrm{d}\Psi}{\mathrm{d}z}+C_5\frac{\mathrm{d}\phi}{\mathrm{d}z} = C_6, \tag{A 14a, b}$$

where

$$C_1 = \frac{\phi}{\sqrt{2\lambda}}-\frac{\phi\epsilon(1-\rho_{\mathrm{G}})}{(2\lambda^2+1)^{\frac{1}{2}}}+\rho_{\mathrm{G}}\,\epsilon\frac{2w_{\mathrm{s}}}{(\lambda^2+1)^{\frac{1}{2}}}+\frac{\rho_{\mathrm{G}}\,\epsilon w_{\mathrm{s}}^2}{\phi}+\kappa\Omega\left[\rho_{\mathrm{G}}\rho_\ell\,\pi^{\frac{1}{2}}\lambda\left(\frac{1}{(\lambda^2+1)^{\frac{1}{2}}}+\frac{w_{\mathrm{s}}}{\phi}\right)\right], \tag{A 15a}$$

$$C_2 = \frac{\Psi}{\sqrt{2\lambda}}-\frac{\Psi\epsilon(1-\rho_{\mathrm{G}})}{(2\lambda^2+1)^{\frac{1}{2}}}-\frac{\Psi\rho_{\mathrm{G}}\,\epsilon w_{\mathrm{s}}^2}{\phi^2}-\kappa\Omega\frac{\rho_{\mathrm{G}}\,\Psi\rho_\ell\,\pi^{\frac{1}{2}}\lambda w_{\mathrm{s}}}{\phi^2}, \tag{A 15b}$$

$$C_3 = \frac{g}{\gamma}\epsilon\frac{\Psi}{\phi}-\frac{\partial\rho_{\mathrm{G}}}{\partial z}\left\{\Psi\epsilon\frac{2w_{\mathrm{s}}}{(\lambda^2+1)^{\frac{1}{2}}}+\frac{\Psi\epsilon}{\phi}w_{\mathrm{s}}^2+\kappa\Omega\left[\Psi\rho_\ell\,\pi^{\frac{1}{2}}\lambda\left(\frac{1}{(\lambda^2+1)^{\frac{1}{2}}}+\frac{w_{\mathrm{s}}}{\phi}\right)\right]+\frac{\Psi\phi\epsilon}{(2\lambda^2+1)^{\frac{1}{2}}}\right\}, \tag{A 15c}$$

$$C_4 = 1-\epsilon\frac{\lambda}{(\lambda^2+1)^{\frac{1}{2}}}-\kappa\Psi\frac{\lambda^2}{(\lambda^2+1)^{\frac{1}{2}}}\rho_{\mathrm{G}}\rho_\ell\,\pi^{\frac{1}{2}}\left(\frac{1}{(\lambda^2+1)^{\frac{1}{2}}}+\frac{w_{\mathrm{s}}}{\phi}\right), \tag{A 15d}$$

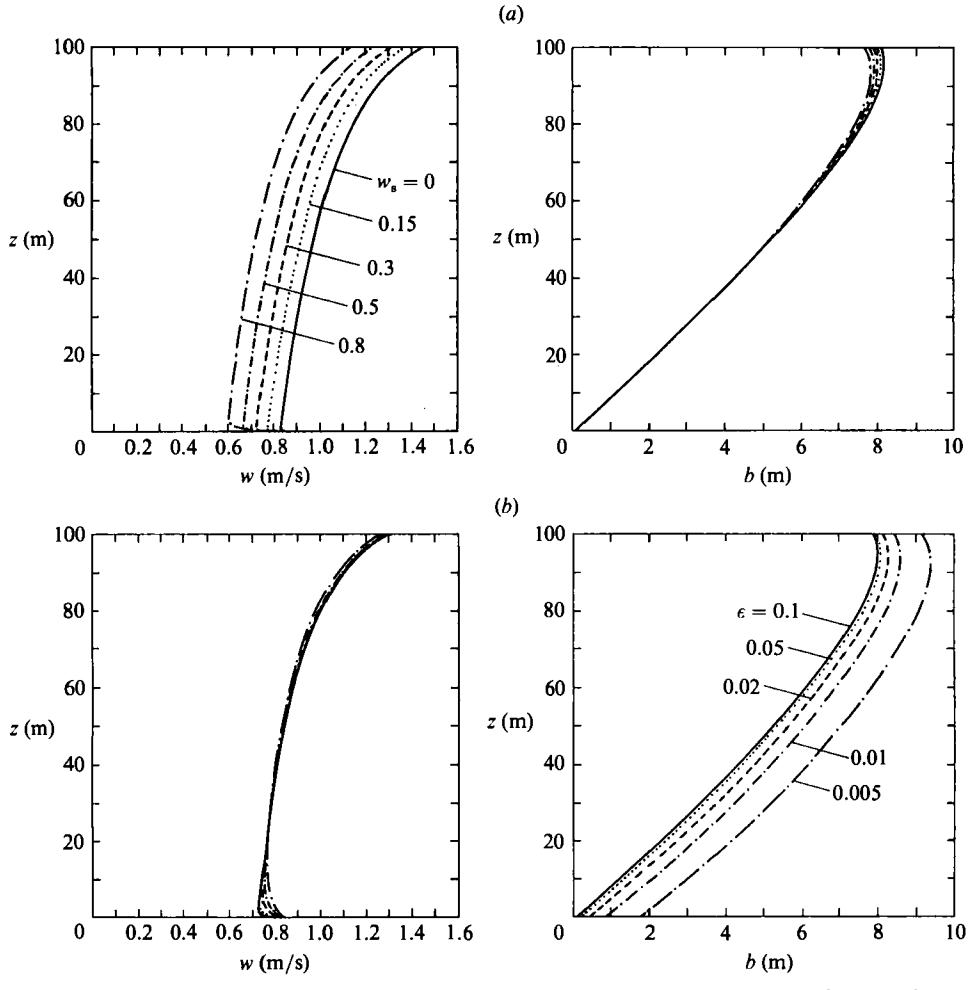

FIGURE 14. Solutions obtained using the similarity solutions as initial conditions showing the effects of (*a*) finite bubble slip, $\epsilon = 0.1$ ($\dot{V}_0 = 0.1$ m^3/s, $\lambda = 0.6$, $\alpha = 0.1$, $\gamma = 1.4$); (*b*) finite void fraction, $w_s = 0.3$ ($\dot{V}_0 = 0.1$ m^3/s, $\lambda = 0.6$, $\alpha = 0.1$, $\gamma = 1.4$).

$$C_5 = \psi^2 \frac{\lambda^2}{(\lambda^2+1)^{\frac{1}{2}}} \kappa \frac{\rho_G \rho_\ell \pi^{\frac{1}{2}} w_s}{\phi^2}, \tag{A 15e}$$

$$C_6 = \frac{2\alpha}{\pi^{\frac{1}{2}}}\phi + \rho_\ell \pi^{\frac{1}{2}} \frac{\lambda^2}{(\lambda^2+1)^{\frac{1}{2}}} \left(\frac{1}{(\lambda^2+1)^{\frac{1}{2}}} + \frac{w_s}{\phi} \right) \kappa \Psi^2 \frac{\mathrm{d}\rho_G}{\mathrm{d}z}. \tag{A 15f}$$

The parameters α, ϵ, λ, w_s are considered to be known (empirical) constants.

The variables ϕ, ψ are functions of z, and the symbols κ and Ω are shorthand for

$$\kappa = -\frac{\dot{m}_g}{\left[\rho_\ell \rho_G \pi^{\frac{1}{2}} \lambda \Psi \left(\frac{1}{(\lambda^2+1)^{\frac{1}{2}}} - \frac{w_s}{\phi} \right) \right]^2},$$

$$\Omega = \frac{\Psi\phi(\rho_G - 1)}{(2\lambda^2+1)^{\frac{1}{2}}} + \Psi\rho_G \frac{2w_s}{(\lambda^2+1)^{\frac{1}{2}}} + \frac{\Psi\rho_G}{\phi} w_s^2.$$

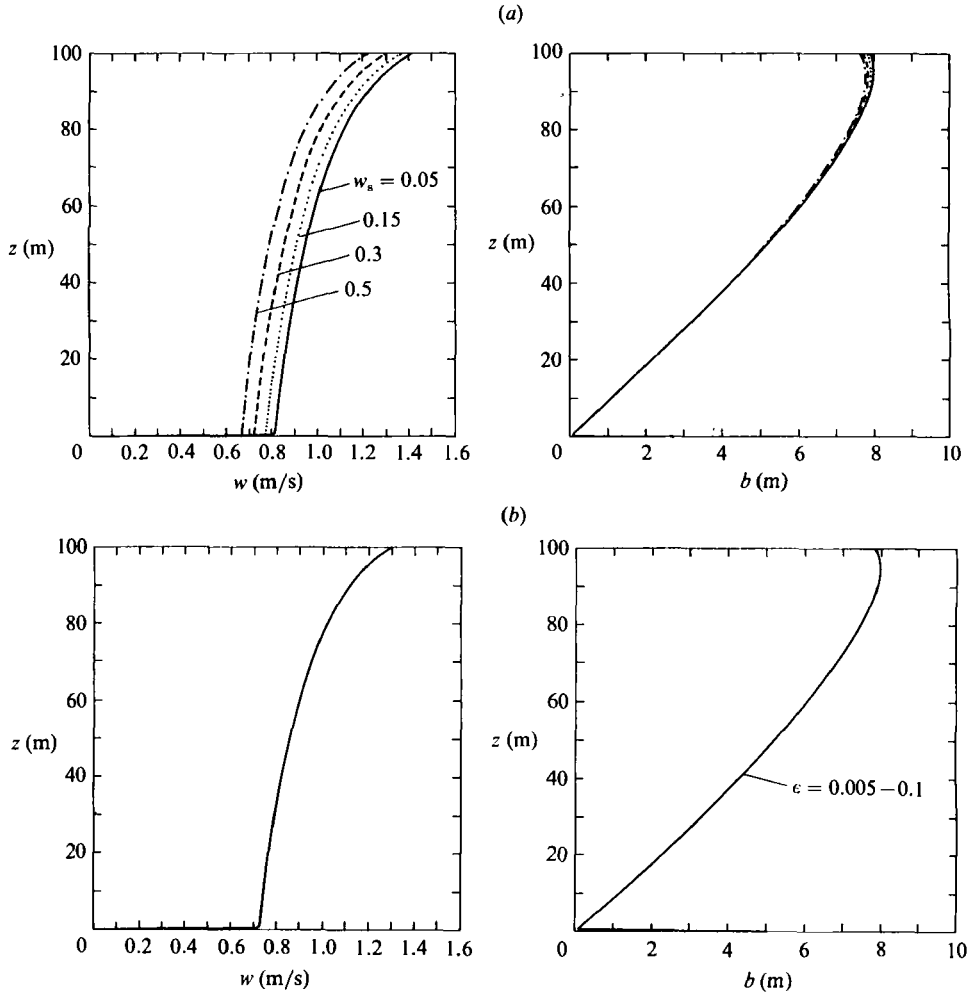

FIGURE 15. Solutions obtained using zero mean velocity and radius from (A 8) as initial conditions showing the effect of (*a*) finite bubble slip, $\epsilon = 0.1$ ($\dot{V}_0 = 0.1$ m^3/s, $\lambda = 0.6$, $\alpha = 0.1$, $\gamma = 1.4$); (*b*) finite void fraction, $w_s = 0.3$ ($\dot{V}_0 = 0.1$ m^3/s, $\lambda = 0.6$, $\alpha = 0.1$, $\gamma = 1.4$).

It remains to specify the initial conditions. These will, in general, depend on the mode of release. The plume equations are not valid in the zone of flow establishment and no solution or accepted flow model for this region are known. It is fortunate that the solution for the established plume flow is rather insensitive to the initial conditions as demonstrated by Milgram (1983).

For practical applications, two plausible choices are available: (i) we assume that the bubble slip vanishes and the gas fraction is small ($\epsilon \ll 1$) near the source so that the similar solution (4*a*, *b*) can be used as starting values (finite bubble-acceleration time); (ii) the mean velocity vanishes near the source, the initial radius is given by (A 8) with $w_m = 0$ for specified flow rate and gas fraction (finite mean-flow acceleration time).

Figure 14(*a*, *b*) shows the results obtained for a wide range of slip velocities w_s and gas fractions ϵ when the similarity solution is used as initial conditions. Figure 15(*a*, *b*) illustrates the effect of the second alternative, again for a wide range of slip

velocities and gas fractions. For reasonable combinations of ϵ and w_s the differences are small, as noted by Milgram.

The plume radius is virtually unaffected for a wide range of slip velocities, w_s = 0–0.8 m/s, whereas the mean plume velocity is slightly changed. For the two values $w_s = 0$ and 0.3 m/s, the correction for slip amounts to about 5% for the range of depths considered. This demonstrates that the similarity solution in §3.1 has adequate accuracy for practical applications, in view of the uncertainty in the empirical parameters and source conditions.

REFERENCES

ABRAMOVICH, G. W. 1963 *The Theory of Turbulent Jets*, pp. 444–474. The MIT Press.

ANDREOPOULOS, J., PRATURI, A & RODI, W. 1986 Experiments on vertical plane buoyant jets in shallow water. *J. Fluid Mech.* **168**, 305–336.

BRENNER, G. & LAGHI, M. 1987 Weitere Untersuchungen über zweidimensionale Blasenplumes. Diplomarbeit in Fluiddynamik, ETH Zürich.

BULSON, P. S. 1963 Large scale bubble breakwater experiments. *Dock and Harbour Authority, London*, Vol. XII, No. 516, Oct. 1963, pp. 191–197.

BULSON, P. S. 1968 The theory and design of bubble breakwaters. *Proc. 11th Conf. Coastal Eng, London*, vol. 2, pp. 995–1015.

FANNELØP, T. K. & SJØEN, K. 1980 Hydrodynamics of underwater blowouts. *AIAA 8th Aerospace Sciences Meeting, January 14–16, Pasadena, California. AIAA paper* 80-0219.

GOOSSENS, L. K. 1979 Reservoir destratification with bubble columns. Thesis, Delft University Press.

HIRSCHBERG, S. 1985 Theoretische und experimentelle Studien über zweidimensionale Blasenplumes. Diplomarbeit in Fluiddynamik, ETH Zürich.

HÜSLER, S. 1988 Untersuchungen über einen nach oben gerichteten, zweidimensionalen Freistrahl im Wasser. Diplomarbeit in Fluiddynamik, ETH Zürich.

IAMANDI, C. & ROUSE, H. 1969 Jet-induced circulation and diffusion. *J. Hydraul. Div. ASCE* **94**, (HY 2), 589–601.

JIRKA, G. H. 1982 Turbulent buoyant jets in shallow fluid layers. In *Turbulent Buoyant Jets and Plumes* (ed. W. Rodi). Pergamon.

JIRKA, G. H. & HARLEMAN, D. R. F. 1979 Stability and mixing of a vertical plane buoyant jet in confined depths. *J. Fluid Mech.* **94**, 275–304.

LAUNDER, B. E. & RODI, W. 1983 The turbulent wall jet—Measurements and modeling. *Ann. Rev. Fluid Mech.* **15**, 429–459.

LEITCH, A. M. & BAINES, W. D. 1989 Liquid volume flux in a weak bubble plume. *J. Fluid Mech.* **205**, 77–98.

MCGUIRK, J. & RODI, W. 1977 A mathematical model for a vertical jet discharging into a shallow lake. *Proc. 17th IAHR-Congress, Paper* A72.

MILGRAM, J. H. 1983 Mean flow in round bubble plumes. *J. Fluid Mech.* **133**, 345–376.

MILGRAM, J. H. & BURGESS, J. J. 1984 Measurements of the surface flow above round bubble plumes. *Appl. Ocean Res.* **6**, 40–44.

SJØEN, K. 1983 Modelling of bubble plumes from subsea blowouts. Dissertation, Norwegian Institute of Technology, University of Trondheim, Division of Aero- and Gas Dynamics.

TAYLOR, G. I. 1955 The action of a surface current, used as a breakwater. *Proc. R. Soc. Lond.* A **231**, 466–478.

TEKELI, S. & MAXWELL, W. H. C. 1978 Behaviour of air bubble screens. *Rep.* UILU-ENG.-74-2019, Dept. Civil Engng, University of Illinois, Urbana-Champaign.

TOPHAM, D. R. 1975*a* Hydrodynamics of an oil well blowout. *Beaufort Sea Tech. Rep.* 33.

TOPHAM, D. R. 1975*b* Measurements of deepset bubble plumes. *Institute of Ocean Sciences, Sidney B.C.* (unpublished).